Thin-Walled Structures 127 (2018) 17–30

Contents lists available at ScienceDirect

Thin-Walled Structures

journal homepage: www.elsevier.com/locate/tws

Full length article

# Assessing the performances of elastic-plastic buckling and shell-solid combination in finite element analysis on plated structures with and without idealised corrosion defects

Y. Wang[a,b,*], J. Downes[a,b], J.A. Wharton[c], R.A. Shenoi[a,b]

[a] Fluid Structure Interactions Group, University of Southampton, Southampton, UK
[b] Southampton Marine and Maritime Institute, University of Southampton, Southampton, UK
[c] National Centre of Advanced Tribology at Southampton, University of Southampton, Southampton, UK

ARTICLE INFO

*Keywords:*
Finite element method
Digital image correlation
Buckling
Model coupling
Corrosion

ABSTRACT

Ships and offshore structures operate in harsh and corrosive environments and they are subject to high hydrodynamic and inertial loads. Thus it is important to accurately predict the mechanical response of thin-walled marine structures subject to corrosion damage in loaded conditions. This paper present a transition study to investigate in depth the usage of shell and solid elements in nonlinear finite element structural analysis with localised corrosion features. An experimental, stereo full field imaging technique, 3D digital image correlation is used to verify both the shell and solid modelling results. The solid-to-shell coupling techniques were subsequently assessed based on a deck plate model. Models containing a localised section using either the second-order hexahedral element C3D20 or tetrahedral element C3D10I show a similar performance that is compatible with the model using only shell element. The proposed coupling method works well for localised electrochemical or mechanical-electrochemical analysis with subsequent geometrical updates.

## 1. Introduction

Corrosion damage accumulation in association with thin-walled structural resilience in marine environments has been an area of study over the last few decades [1–3]. The accuracy of the structural analysis can directly affect reliability prediction and maintenance or repair strategies [4]. Depending on the structural location, material properties, and the service environment, corrosion damage either can spread over the entire plating, become localised in regions that are associated with a failed protection system (i.e., polymeric coating defects or cathodic protection problems) or be linked to complex geometrical surfaces including weld imperfections. Fig. 1 shows an example of such an imperfection along a butt weld. Rough surfaces due to corrosion and rust can be potential stress concentration sites and thus a threat to structural reliability [5–7]. To assess these corrosion effects, numerous studies have been undertaken on plated or tubular marine structures containing representative corrosion features [3,8–14]. Among the limited analysis approaches, the finite element method with fully nonlinear material and geometric properties is commonly used to predict ultimate strength capacity primarily for small scale or individual structural members with corrosion damage. Many finite element analysis (FEA) models use a two-dimensional (2D) 4-node shell element to simulate structures which require modelling of sections of plating, box girders and hull girders. In these scenarios, the corrosion damage is normally idealised as a uniform thickness reduction especially for hull girder and platform simulations [15–19]. Smaller models with local thickness variations have also been studied where different section properties need to be assigned to shell elements [3,10,20]. Verifications by both laboratory and practical experience have shown that under appropriate boundary conditions and hourglass control, shell elements are capable of accurately predicting the ultimate strength of intact plated structures at low computational cost and with less modelling effort [4,8,21,22]. In comparison, models built by either three-dimensional (3D) solid elements show an enhanced ability to simulate more realistic corrosion topographies [6,23]. Surface mapping tools can be used to transfer actual corroded surface features directly to a 3D model [9,23–25]. Therefore, detailed stress and strain distributions can be obtained for the surface. However, shear and volume locking may occur in such models that prevent thin-walled structure behaviour. The high computational cost also indicates that it is almost impossible to use solid models for rapid strength prediction of ship hulls or offshore platforms practically [26,27].

Alternatively, for marine structures with 15–20 years of operational service, the accumulation and evolution of corrosion damage will result

* Corresponding author at: Fluid Structure Interactions Group, University of Southampton, Southampton Marine and Maritime Institute, Southampton, UK.
*E-mail address:* yw4u14@soton.ac.uk (Y. Wang).

https://doi.org/10.1016/j.tws.2018.01.030
Received 20 July 2017; Received in revised form 11 January 2018; Accepted 24 January 2018
0263-8231/ 

**Nomenclature**

| | |
|---|---|
| $a$ | Length of the deck plate model / mm |
| $b$ | Width of the deck plate model / mm |
| $C$ | Correlation function |
| $d_p$ | Position tolerance for the surface-based approach / mm |
| $\boldsymbol{e}_i$ | Current configuration base vector (regardless of rotation constraint at the slave node) |
| $E$ | Young's modulus / GPa |
| $F$ | Grey value matrix of reference image |
| $\boldsymbol{F}^{\mathrm{Shell}}$ | Force distribution at the reference shell node |
| $\boldsymbol{F}_{\mathrm{i}}^{\mathrm{Solid}}$ | Force distribution at the coupling solid node $i$ |
| $G$ | Grey value matrix of deformed image |
| $\boldsymbol{I}$ | Second-order identity tensor |
| $k$ | Smallest integral satisfying $a/b \le \sqrt{k(k+1)}$ |
| $m$ | Pixel location in the reference image |
| $\boldsymbol{M}^{\mathrm{Shell}}$ | Moment at the reference shell node |
| $n$ | Pixel location in the reference image |
| $\boldsymbol{n}$ | Normal direction of the deformed solid configuration |
| $N$ | Subset size |
| $\boldsymbol{N}$ | Normal direction of the reference solid configuration |
| $\boldsymbol{r}_{\mathrm{i}}$ | Influence distance at the coupling solid node $i$ for the surface-based approach / mm |
| $\boldsymbol{R}(\boldsymbol{\phi}^{\mathrm{m}})$ | Rotation matrix associated with the master node rotation $\boldsymbol{\phi}^{\mathrm{m}}$ |
| $\boldsymbol{S}$ | Skew symmetric matrix form of the rotation vector $\boldsymbol{\phi}$ |
| $t_p$ | Thickness of the deck plate model / mm |
| $\boldsymbol{T}$ | Coupling node arrangement inertia tensor |
| $u$ | Displacement of the subset centre from the reference image to the deformed image / mm |
| $\boldsymbol{u}^{\mathrm{Shell}}$ | Displacement of the shell node |
| $\boldsymbol{u}_i^{\mathrm{Solid}}$ | Displacement of the solid node $i$ |
| $v$ | Displacement of the subset centre from the reference image to the deformed image / mm |
| $w_i$ | Weighing factor at solid node $i$ |
| $\overline{w}_{\mathrm{i}}$ | Nominalised weight factor |
| $w_p$ | Deck plate initial deflection |
| $\boldsymbol{x}^{\mathrm{m}}$ | Deformed configuration position of master node |
| $\overline{\boldsymbol{x}}^{\mathrm{s}}$ | Fully constrained slave node position |
| $\boldsymbol{x}^{\mathrm{s}}$ | Partially constrained slave node position |
| $\boldsymbol{x}^{\mathrm{Shell}}$ | Positions of the reference shell node |
| $\boldsymbol{x}_{\mathrm{i}}^{\mathrm{Solid}}$ | Positions of the coupling solid node $i$ |
| $\boldsymbol{X}^{\mathrm{s}}$ | Reference configuration positions of the slave node |
| $\boldsymbol{X}^{\mathrm{m}}$ | Reference configuration positions of the master node |
| $y_i$ | Translation degree of freedom $i$ at the additional node / mm |
| $\beta$ | Slenderness ratio |
| $\nu$ | Poisson ratio |
| $\sigma_y$ | Yield stress of the material / MPa |
| $\boldsymbol{\phi}$ | Rotation vector |
| $\boldsymbol{\phi}^{\mathrm{m}}$ | Master node rotation |

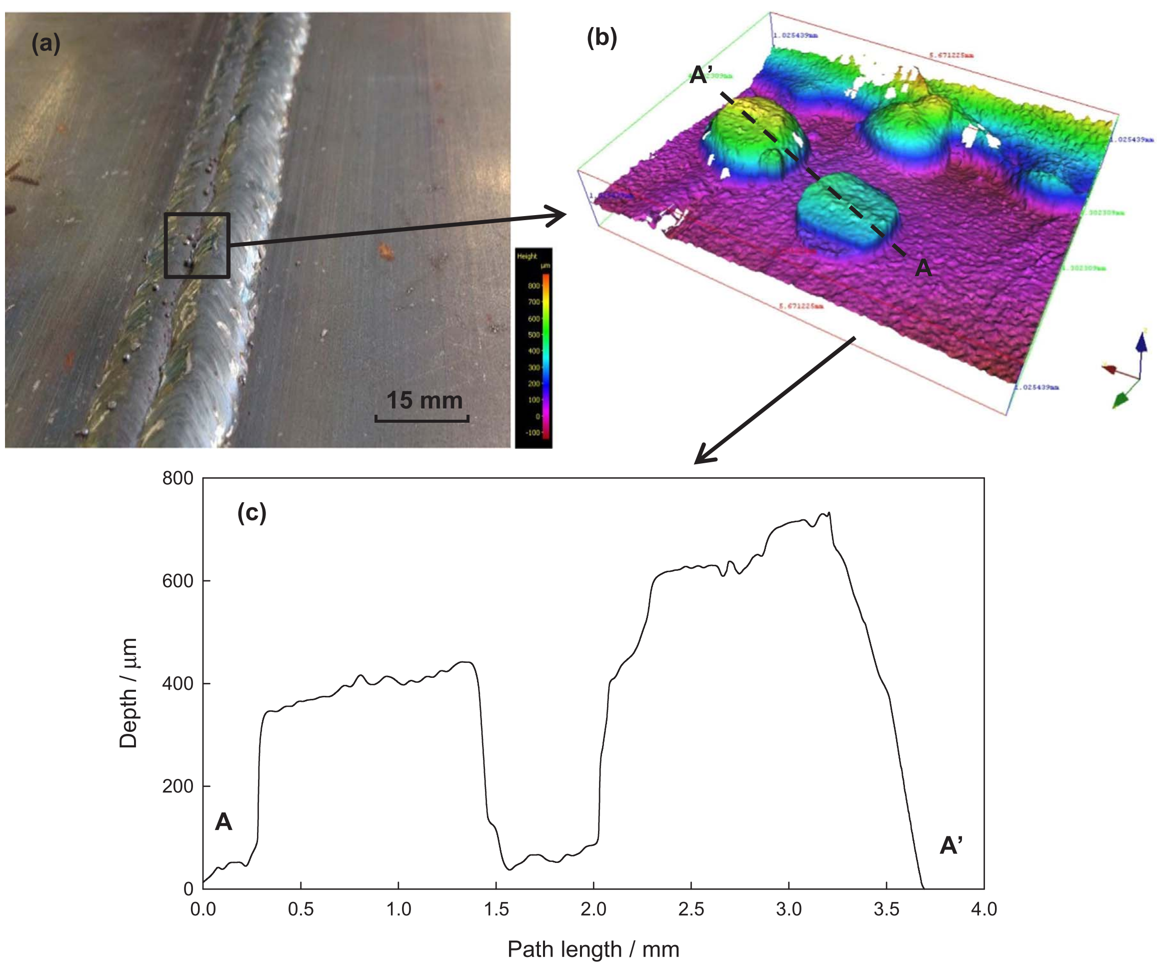


**Fig. 1.** Imperfections on the butt welds of a shipping grade steel plate: (a) welded plate sample; (b) three-dimensional surface profilometry (scan area: 5.7 mm × 4.3 mm); and (c) profile between A-A′.